

Stabilized Pair Density Wave via Nanoscale Confinement of Superfluid ^3He

A.J. Shook,¹ V. Vadakumbatt,¹ P. Senarath Yapa,¹ C. Doolin,¹ R. Boyack,^{1,2} P.H. Kim,¹ G.G. Popowich,¹ F. Souris,¹ H. Christani,¹ J. Maciejko,^{1,2,*} and J.P. Davis^{1,†}

¹*Department of Physics, University of Alberta, Edmonton, Alberta T6G 2E1, Canada*

²*Theoretical Physics Institute, University of Alberta, Edmonton, Alberta T6G 2E1, Canada*

(Dated: November 25, 2021)

Superfluid ^3He under nanoscale confinement has generated significant interest due to the rich spectrum of phases with complex order parameters that may be stabilized. Experiments have uncovered a variety of interesting phenomena, but a complete picture of superfluid ^3He under confinement has remained elusive. Here, we present phase diagrams of superfluid ^3He under varying degrees of uniaxial confinement, over a wide range of pressures, which elucidate the progressive stability of both the A -phase, as well as a growing region of stable pair density wave (PDW) state.

While bulk superfluid ^3He is exceptionally well understood, both theoretically and experimentally [1], much is unknown when confinement approaches the scale of the superfluid coherence length. In the bulk, only two phases are stable, the so-called A and B phases. The A -phase—with nodes in the gap, as shown in Fig. 1(a)—is stabilized by strong coupling effects at high pressures [2], whereas the B -phase—with its isotropic gap—dominates the phase diagram (Fig. 4(a)). When confined via engineered structures, the phase diagram is expected to be altered significantly. Due to the unconventional p -wave pairing in ^3He , non-magnetic scattering at surfaces is sufficient to break Cooper pairs. Thus surface scattering serves to distort and suppress the order parameter. In fact, under confinement the B -phase is altered to become the planar-distorted B -phase, see Eq. (3), with a suppressed gap at antipodal points on the Fermi surface (Fig. 1(a)). Early experiments to explore the effects of confinement resulted in a variety of observations, including hints of a new phase transition [3], the complete elimination of the B -phase in favor of the A -phase [4], and modification of the relative stability of the A and B -phases [5, 6].

It was realized by Vorontsov and Sauls that order parameter suppression due to surface scattering could be minimized by the formation of domain walls between two orientations of planar-distorted B -phases, Fig. 1(b), when the confinement lies in a particular range of length scales [7]. Alignment of these domain walls was later predicted to form the basis of an ordered superfluid phase, deemed the stripe phase [8]. The stripe phase is an example of a pair density wave (PDW), a state that breaks both gauge and translational symmetries and is now believed to play an important role in the cuprate superconductors [9]. The observation of such a PDW state in superfluid ^3He could lead to a deeper understanding of this state, and influence understanding of PDWs in unconventional superconductors.

The prediction of Vorontsov and Sauls stimulated numerous experimental searches, including nuclear magnetic resonance (NMR) [10, 11], shear micromechanical

resonators [12], and torsional oscillators [13]—with spatial confinements of 700 nm [10], 1.1 μm [11, 13], and 1.25 μm [12]. Most conclusively, NMR studies have simultaneously observed signals from two different planar-distorted B -phases. Despite this observation, they have concluded that their measurements are inconsistent with the stripe phase, and instead have suggested another PDW with soft domain walls between localized puddles of planar-distorted B -phase, which they have termed the polka-dot phase [11]. To date, it is unclear if these results represent the true thermodynamic phase diagram of superfluid ^3He under uniform confinement, or if they remain complicated by non-uniformities in the structures, e.g., bowing induced by pressurization. Here, in an effort to resolve this question, we use microfabricated fourth-sound resonators [14, 15], which are sensitive indicators of the superfluid fraction, to explore the generation of

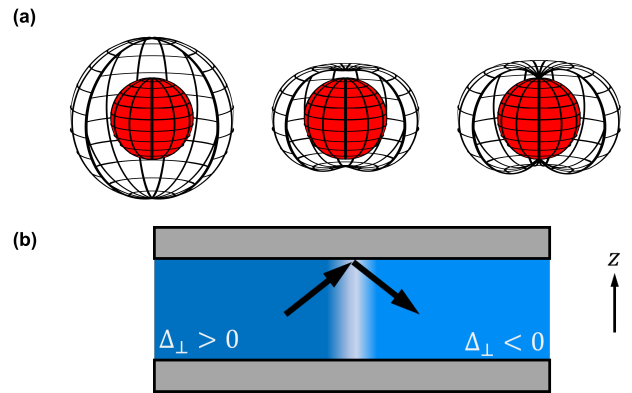


FIG. 1. (a) Schematic momentum-space representations of the quasiparticle gaps for the relevant superfluid states under planar confinement: from left to right, the isotropic B -phase, the planar distorted B -phase, and the A -phase. (b) Confinement along the z -axis. When Cooper pairs scatter off a wall the z -component Δ_{\perp} of the order parameter changes sign, which for the planar-distorted B -phase causes pair breaking. This can be minimized by the formation of domain walls between regions of planar-distorted B -phase with alternating signs of Δ_{\perp} . A regular arrangement of these domain walls leads to broken translational symmetry and the PDW state.

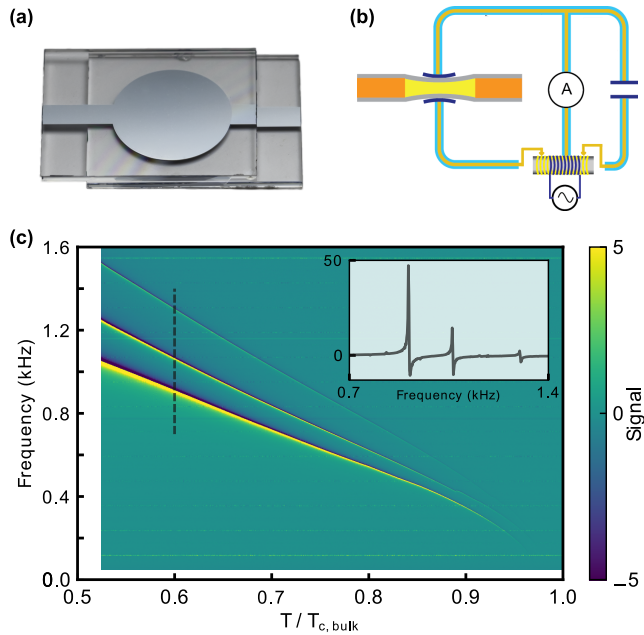


FIG. 2. Experimental system and superfluid Helmholtz resonator frequency data. (a) Helmholtz resonator, fabricated out of single-crystal quartz etched to define the nanoscale confinement, then deposited with aluminum inside the etched area. (b) Under an applied voltage the electrodes are slightly displaced towards each other, pushing the superfluid ^3He out of the channel and exciting the Helmholtz mode. This is detected using a capacitance bridge that outputs a current that is digitized. (c) Three Helmholtz resonators, with varying confinement, are wired in parallel and measured simultaneously using a chirped pulse scheme described in the text. Due to the measurement configuration the resonances appear Fano-like, yet are easily resolved, as shown in the inset—corresponding to the cross-section marked with the dashed line in the main panel.

spatial order in superfluid ^3He . These devices are fully immersed in liquid and therefore are mechanically unaffected by pressurization of the ^3He . This allows us to explore the phase diagram up to 28 bar, revealing signatures of PDW in the phase diagram that have never been observed. Furthermore, we simultaneously measure three devices with varying degrees of confinement, in order to map the effect of confinement on the stability of the PDW state.

The devices used to probe the superfluid phases under confinement, shown in Fig. 2(a), are microfabricated from single-crystal quartz, with similar devices having been previously demonstrated to selectively probe the superfluid fraction within a nanoscale channel of ^4He [14]. They work by exciting a mechanical resonance in the fluid upon excitation by a voltage source, Fig. 2(b). This causes a deflection of the two electrodes—on opposite sides of the nanoscale cavity—via a strong electrostatic force due to the small gap between the electrodes. As a result of the deflection, fluid in the nanoscale channels is

pushed out, which—when driven on resonance—excites a Helmholtz mechanical mode. In the devices measured here, with channel depths of 636 ± 12 nm, 805 ± 4 nm, and 1067 ± 7 nm, the normal fluid is viscously clamped [16], hence the frequency ω of the Helmholtz mode is related to the superfluid fraction ρ_s/ρ :

$$\omega^2 = K \left(\frac{\rho_s}{\rho} \right). \quad (1)$$

K represents terms that involve measured geometric factors, and the calibrated spring constant of the plate and helium [14]. In this work, we have extended this to superfluid ^3He by constructing an adiabatic nuclear demagnetization stage and ^3He sample cell, described in Appendix A.

To drive the superfluid mechanical mode, we use a chirped pulse scheme to excite all three devices simultaneously and acquire their response in the time domain [17]. Fast Fourier transforming this time domain data allows us to rapidly acquire the frequency response of the Helmholtz resonators, and enables mapping of their frequencies during adiabatic nuclear demagnetization temperature sweeps. An example at 12.7 bar is shown in

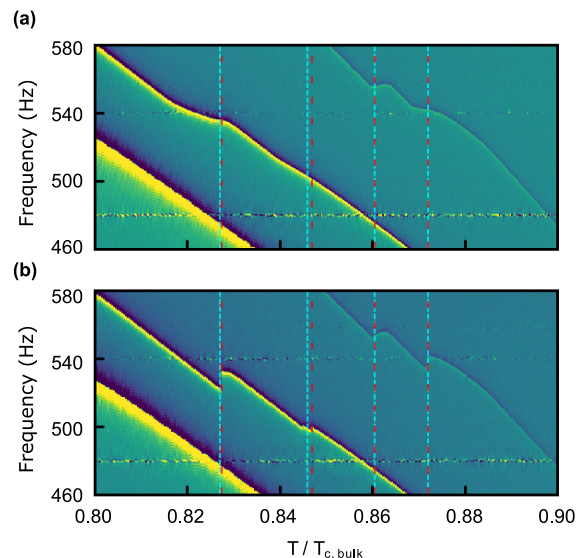


FIG. 3. Zoom-in around phase transitions for 22 bar data. (a) Cooling run with phase transitions in the 1067 nm device (upper trace) and 805 nm device (middle trace) marked with blue dashed lines. (b) Same as in (a) but for a warming run and phase transitions marked with red dashed lines. Note that (a) and (b) are on the same scales and the dashed lines cross both panels to emphasize that there is no significant hysteresis between warming and cooling in our experiments. Observation of two first-order phase transitions demonstrates not only that the PDW state at intermediate temperatures is stable, but the lack of hysteresis points to an intermediate phase between the A and planar distorted B -phases that eliminates supercooling [13, 18].

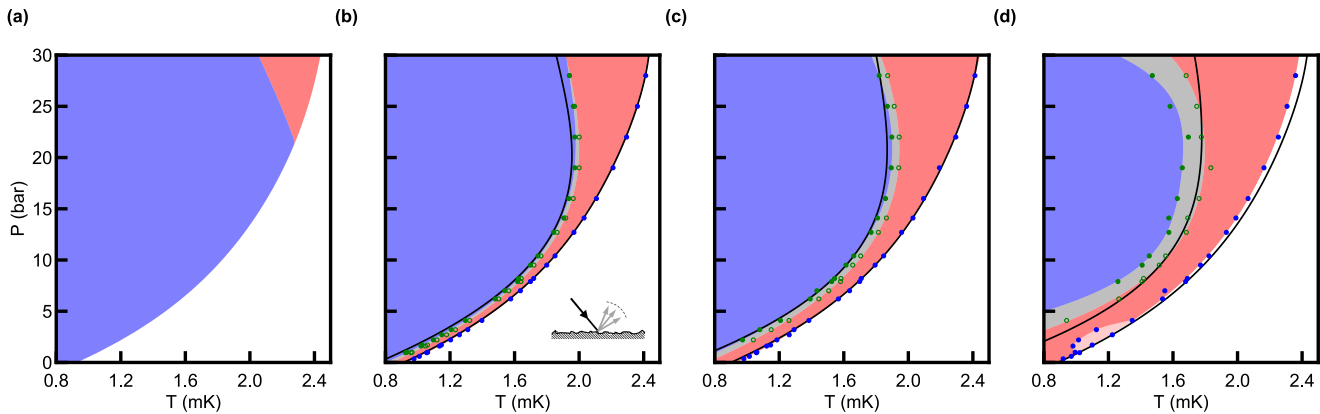


FIG. 4. Pressure (P)-temperature (T) phase diagrams of superfluid ^3He , on warming. (a) Bulk phase diagram shown for reference, with the A -phase (pink) and B -phase (blue). Phase diagrams for (b) 1067 nm, (c) 805 nm, and (d) 636 nm confinements are shown with A -phase (pink) and planar-distorted B -phase (blue). Under confinement, a new phase appears, which we have colored grey. As the confinement increases from left to right, the width of the grey region grows, as does the stability of the A -phase. Ginzburg-Landau calculations, including strong coupling corrections [19, 20] and the effect of confinement [21] with diffuse boundary conditions (illustrated schematically in the inset of (b)), are included as the black curves—without any adjustable parameters. The PDW must lie between the A -phase and the planar distorted B -phase [8, 19], hence the grey region is concluded to be the stable PDW state.

Fig. 2(c). Three superfluid-mechanical resonances are seen, with Fano-like character due to the measurement scheme, as shown in the inset. The highest frequency resonance corresponds to the 1067 nm device and is assumed to have a temperature dependence that is indiscernible from that of the bulk superfluid fraction [22, 23], as was found in Ref. [13]. We use the temperature dependence of the 1067 nm device as a sensitive local secondary thermometer, which is referenced to both a melting curve thermometer on the same experimental stage and a tuning fork [24, 25] immersed in the same sample cell. We note that we have performed sweeps of the drive amplitude, and are in a linear response regime in all measurements. This also serves to verify that our drive does not cause heating of the liquid ^3He .

The temperature dependence of the superfluid fraction is known to be an excellent indicator of phase transitions [13]. We show in Fig. 3 portions of temperature sweeps, at 22 bar, demonstrating two phase transitions per device—suggesting the existence of three stable superfluid phases. This observation is quite startling, not only as there are only two phases observed in bulk ^3He , but also that two distinct first-order phase transitions were not observed in previous NMR or torsional oscillator experiments. Instead, those experiments found a single first-order phase transition that occurred over a broad temperature range [13], which they attributed to inhomogeneous thickness of the superfluid. Recent NMR experiments at low pressure in a 1.1 μm device do not show a broad phase transition, yet also do not observe two first-order phase transitions. This is reasonable, considering the complete phase diagram that we show next.

To determine the phase diagram under confinement,

and the relation between our data and previous observations, we have explored these phase transitions over a wide pressure range, from 0.35 bar to 28 bar, and compiled the thermodynamic warming transitions in Fig. 4. Note, we discuss the lack of hysteresis between warming and cooling below. In panels (b–d) of Fig. 4, the experimentally determined phase transitions are shown as circles: blue for the transition to the normal state, and the open and filled green circles for kinks in the superfluid fraction. Smooth fits to the data points delineate colored regions, and hence regions of stable phases.

To understand these results, we theoretically model the system using a Ginzburg-Landau approach. Superfluid ^3He is a spin-triplet p -wave superfluid characterized by the Cooper pair amplitude

$$\Delta_{\alpha\beta}(\hat{\mathbf{p}}) = A_{\mu j}(i\sigma_{\mu}\sigma_y)_{\alpha\beta}\hat{p}_j \quad (2)$$

between fermions of spin α, β and relative momentum $\hat{\mathbf{p}}$, where $\sigma_x, \sigma_y, \sigma_z$ are the Pauli spin matrices and $A_{\mu j}$ is a 3×3 matrix order parameter. We numerically solve the Ginzburg-Landau equations for $A_{\mu j}$ in a slab geometry following the formalism of Refs. [19, 26] which incorporates confinement effects [21] as well as strong coupling corrections [20]. The depairing effect of surface roughness [27] on the cavity walls is taken into account through diffuse scattering boundary conditions. The order parameter profile is assumed to be z -dependent to account for confinement effects, but translationally invariant in the plane of the device (x - y plane). Two such uniform phases are known to be stabilized under confinement, the

planar-distorted B -phase with order parameter

$$A_{\mu j}^{\text{pdB}}(z) = \begin{pmatrix} \Delta_{\parallel}(z) & 0 & 0 \\ 0 & \Delta_{\parallel}(z) & 0 \\ 0 & 0 & \Delta_{\perp}(z) \end{pmatrix}_{\mu j}, \quad (3)$$

and the A -phase, with order parameter

$$A_{\mu j}^{\text{A}}(z) = \begin{pmatrix} 0 & 0 & 0 \\ 0 & 0 & 0 \\ \Delta(z) & i\Delta(z) & 0 \end{pmatrix}_{\mu j}. \quad (4)$$

Strong coupling corrections are necessary to account for the stability of the A -phase relative to the planar phase, i.e., Eq. (3) with vanishing z -component of the order parameter, $\Delta_{\perp} = 0$.

We include the known bulk phase diagram in Fig. 4(a) for comparison, with the B -phase in blue and the A -phase in pink. The leftmost black curve in panels (b–d) is the calculated phase boundary between the planar-distorted B -phase and the A -phase, while the black curve on the right is the calculated pressure-dependent critical temperature $T_c(P)$. The excellent agreement between theory and experiment in panels (b–c) and to a lesser extent (d), as well as comparison with the bulk phase diagram, unambiguously suggest the blue and pink regions in the phase diagrams under confinement are the planar-distorted B -phase and A -phase, respectively. However, under the assumption of translation invariance in the x - y plane, the Ginzburg-Landau analysis does not capture the experimentally observed grey region that lies between the two uniform phases.

An obvious candidate for this region is thus a spatially inhomogeneous phase exhibiting domain walls across which the z -component Δ_{\perp} of the superfluid order parameter changes sign, see Fig. 1(b). While in bulk ${}^3\text{He}$ such domain walls [28, 29] are not energetically favorable, for device thicknesses D of order the coherence length ξ , the energy cost of creating a domain wall can be compensated by the reduction in gradient energy associated with surface pairbreaking. Everywhere on the domain wall, Δ_{\perp} vanishes due to the change of sign and is thus uniform along the confinement direction, which reduces this energy. For sufficiently thin devices the gain in energy from the reduction in surface pairbreaking outweighs the cost from domain wall surface tension, and domain walls are favored. The enhanced stability of the grey region with increasing degree of confinement, observed in Fig. 4(b–d), thus further supports the interpretation of this region as a spatially inhomogeneous phase. Finally, the stabilization of domain walls in the vicinity of the A - B phase boundary can be understood from the following argument. Upon approaching the A - B phase boundary from the planar-distorted B -phase, Δ_{\perp} is gradually reduced. Deep in the planar-distorted B -phase, suppressing Δ_{\perp} on a domain wall is not energetically favorable, but becomes increasingly so upon approach to the transition. In the A -phase, $\Delta_{\perp} = A_{zz}$ is uniformly zero due

to the different symmetry of the phase, see Eq. (4), thus surface pairbreaking is automatically minimized without the need for domain walls.

While this argument alone cannot predict the optimal spatial arrangement of domain walls, previous studies strongly suggest periodic patterns of ordering are favored. Explicit calculations [8, 19, 30] using either quasiclassical Green's functions or the Ginzburg-Landau approach, and for a variety of boundary conditions ranging from specular to maximally pairbreaking, indicate a periodic arrangement of domain walls forming a unidirectional PDW phase (stripe phase) can be stabilized at low pressures under confinement near the A - B phase boundary for slab thicknesses $D \sim 10\xi$. However, NMR studies [11] favor an interpretation in terms of a two-dimensional PDW phase—the polka-dot phase—with the symmetry of a square or triangular lattice. In the pressure range 0–15 bar the PDW phase appears in our devices in a temperature range such that $8 \lesssim D/\xi \lesssim 18$, in broad agreement with theory expectations for the stripe phase, but unexpectedly persists at pressures up to 30 bar, at least in the two thinnest devices.

Our current experiments cannot resolve the stripe/polka-dot debate, but do indicate that the PDW state observed here is thermodynamically stable from the fact that it is seen reproducibly both on warming and on cooling, as shown for example in Fig. 3. It is also noteworthy that we observe no significant hysteresis in the phase transitions between the A -phase and the PDW state, nor between the PDW state and the planar-distorted B -phase, despite the fact that these are first-order phase transitions for which supercooling would be expected—especially as significant supercooling between the A and B -phases is routinely observed in bulk ${}^3\text{He}$. The lack of hysteresis is consistent with recent torsional oscillator experiments [13]. In that work, the existence of an unseen spatially modulated phase was suggested to account for the lack of hysteresis. This can be understood by the presence of an intermediate phase between the A and B -phases (the PDW) lowering the nucleation barrier between these states [18].

Finally, we note that we have observed an anomalous region in the 636 nm device between pressures of 0.95–4.10 bar, as seen in the light pink region of Fig. 4(d). Whereas the rest of our phase transitions are fully reproducible, in this region we find that on some runs we observe transitions to the A -phase as expected, yet on occasion we find that the transition occurs at a reduced temperature. Further experiments are required to elucidate the behavior of this region and will be the subject of future work.

In conclusion, we have mapped the phase diagrams of superfluid ${}^3\text{He}$ under nanoscale confinement and have demonstrated the existence of a thermodynamically-stable PDW state, breaking both gauge and translational symmetry. The stability of both the A -phase and

the PDW state grow with increasing confinement, consistent with, and serving to reconcile, previous experiments, e.g., the stabilization of the *A*-phase with increasing confinement in Refs. [4–6]. Nonetheless, questions remain. What is the nature of the anomalous region at low pressure in the 636 nm device? Furthermore, as the Helmholtz resonators excite longitudinal (fourth) sound, can we use these to find spectroscopic signatures of the PDW, i.e., order-parameter collective modes [31]? Finally, our Helmholtz resonators may be capable of observing evidence of Majorana fermions associated with Andreev bound states at surfaces [23, 32–35] and at the domain walls that make up the PDW observed here, through the superfluid fraction [23] or collective modes [36, 37]—a tantalizing possibility for future experiments.

Authors acknowledge useful conversations with J.A. Sauls, and thank W.P. Halperin and Y. Lee for generous assistance with melting curve thermometry. This work was supported by the University of Alberta, Faculty of Science and Theoretical Physics Institute; the Natural Sciences and Engineering Research Council, Canada (Grants Nos. RGPIN-04523-16, RGPIN-2014-4608, DAS-492947-16, and CREATE-495446-17); the Canada Foundation for Innovation; the Canada Research Chair Program; and the Canadian Institute for Advanced Research. A.S. and V.V. contributed equally to this work.

APPENDIX A: LOW-TEMPERATURE SETUP

Our low-temperature setup consists of an adiabatic nuclear demagnetization stage, incorporated into a commercial dilution fridge. The nuclear stage was made from high-purity copper, and vacuum annealed after machining. The copper stage is attached to the microkelvin plate, where the experimental cell and melting curve thermometer are mounted, via a superconducting heat switch made of high-purity indium wires. The sample cell housing the liquid ^3He and Helmholtz resonators is designed after Ref. [38], with sintered copper powder heat exchangers [39] of total surface area 84 m^2 . With ^4He impurities of 1% in our ^3He , this results in a surface coverage of $\approx 1/4$ of a monolayer, consistent with diffuse boundary scattering [4] and the results of our Ginzburg-Landau calculations.

* maciejko@ualberta.ca

† jdavis@ualberta.ca

- [1] D. Vollhardt and P. Wölfle, *The Superfluid Phases of Helium 3* (Dover Publications, Mineola, NY, 2013).
 [2] D. Rainer and J.W. Serene, *Phys. Rev. B* **13**, 4745 (1976).
 [3] J. Xu and B.C. Crooker, *Phys. Rev. Lett.* **65**, 3005 (1990).

- [4] M.R. Freeman and R.C. Richardson, *Phys. Rev. B* **41**, 11011 (1990).
 [5] S. Miyawaki, K. Kawasaki, H. Inaba, A. Matsubara, O. Ishikawa, T. Hata, and T. Kodama, *Phys. Rev. B* **62**, 5855 (2000).
 [6] K. Kawasaki, T. Yoshida, M. Tarui, H. Nakagawa, H. Yano, O. Ishikawa, and T. Hata, *Phys. Rev. Lett.* **93**, 105301 (2004).
 [7] A.B. Vorontsov and J.A. Sauls, *J. Low Temp. Phys.* **138**, 283 (2005).
 [8] A.B. Vorontsov and J.A. Sauls, *Phys. Rev. Lett.* **98**, 045301 (2007).
 [9] D.F. Agterberg, J.C. Séamus Davis, S.D. Edkins, E. Fradkin, D.J. Van Harlingen, S.A. Kivelson, P.A. Lee, L. Radzihovsky, J.M. Tranquada, and Y. Wang, arXiv:1904.09687.
 [10] L.V. Levitin, R.G. Bennett, A. Casey, B. Cowan, J. Saunders, D. Drung, Th. Schurig, and J.M. Parpia, *Science* **340**, 841 (2013).
 [11] L.V. Levitin, B. Yager, L. Sumner, B. Cowan, A.J. Casey, J. Saunders, N. Zhelev, R.G. Bennett, and J.M. Parpia, *Phys. Rev. Lett.* **122**, 085301 (2019).
 [12] P. Zheng, W.G. Jiang, C.S. Barquist, Y. Lee, and H.B. Chan, *Phys. Rev. Lett.* **117**, 195301 (2016).
 [13] N. Zhelev, T.S. Abhilash, E.N. Smith, R.G. Bennett, X. Rojas, L. Levitin, J. Saunders, and J.M. Parpia, *Nat. Commun.* **8**, 15963 (2017).
 [14] X. Rojas and J.P. Davis, *Phys. Rev. B* **91**, 024503 (2015).
 [15] F. Souris, X. Rojas, P.H. Kim, and J.P. Davis, *Phys. Rev. Applied* **7**, 044008 (2017).
 [16] H. Kojima, D.N. Paulson, and J.C. Wheatley, *J. Low Temp. Phys.* **21**, 283 (1975).
 [17] C. Doolin, Ph.D. thesis, University of Alberta, 2019.
 [18] S.-H. Henry Tye and D. Wohms, *Phys. Rev. B* **84**, 184518 (2011).
 [19] J.J. Wiman and J.A. Sauls, *J. Low Temp. Phys.* **184**, 1054 (2016).
 [20] H. Choi, J.P. Davis, J. Pollanen, T. M. Haard, and W. P. Halperin, *Phys. Rev. B* **75**, 174503 (2007).
 [21] Y.-H. Li and T.-L. Ho, *Phys. Rev. B* **38**, 2362 (1988).
 [22] J.M. Parpia, D.G. Wildes, J. Saunders, E.K. Zeise, J.D. Reppy, and R.C. Richardson, *J. Low Temp. Phys.* **61**, 337 (1985).
 [23] H. Wu and J.A. Sauls, *Phys. Rev. B* **88**, 184506 (2013).
 [24] R. Blaauwgeers, M. Blazkova, M. Človečko, V.B. Eltsov, R. de Graaf, J. Hosio, M. Krusius, D. Schmoranzner, W. Schoepe, L. Skrbek, P. Skybam, R.E. Solntsev, and D.E. Zmeev, *J. Low Temp. Phys.* **146**, 537 (2007).
 [25] D.C. Carless, H.E. Hall, and J.R. Hook, *J. Low Temp. Phys.* **50**, 605 (1983).
 [26] J.J. Wiman and J.A. Sauls, *Phys. Rev. B* **92**, 144515 (2015).
 [27] V. Ambegaokar, P.G. de Gennes, and D. Rainer, *Phys. Rev. A* **9**, 2676 (1974).
 [28] M.M. Salomaa and G.E. Volovik, *Phys. Rev. B* **37**, 9298 (1988).
 [29] M. Silveri, T. Turunen, and E. Thuneberg, *Phys. Rev. B* **90**, 184513 (2014).
 [30] K. Aoyama, *J. Phys. Soc. Jpn.* **85**, 094604 (2016).
 [31] J.P. Davis, H. Choi, J. Pollanen, and W.P. Halperin, *Phys. Rev. Lett.* **97**, 115301 (2006).
 [32] G.E. Volovik, *JETP Lett.* **90**, 398 (2009).
 [33] S.B. Chung and S.C. Zhang, *Phys. Rev. Lett.* **103**, 235301 (2009).

- [34] J.P. Davis, J. Pollanen, H. Choi, J.A. Sauls, W.P. Halperin, and A.B. Vorontsov, *Phys. Rev. Lett.* **101**, 085301 (2008).
- [35] S. Murakawa, Y. Wada, Y. Tamura, M. Wasai, M. Saitoh, Y. Aoki, R. Nomura, Y. Okuda, Y. Nagato, M. Yamamoto, S. Higashitani, and K. Nagai, *J. Phys. Soc. Jpn.* **80**, 013602 (2011).
- [36] Y.J. Park, S.B. Chung, and J. Maciejko, *Phys. Rev. B* **91**, 054507 (2015).
- [37] T. Mizushima and J.A. Sauls, arXiv:1801.02277.
- [38] J. Pollanen, Ph.D. thesis, Northwestern University, 2012.
- [39] M. Krusius, D.N. Paulson, and J.C. Wheatley, *Cryogenics* **18**, 649 (1978).